State-of-Charge (SOC)-Balancing Control of a Battery Energy Storage System Based on a Cascade PWM Converter

Laxman Maharjan, *Student Member, IEEE*, Shigenori Inoue, *Member, IEEE*, Hirofumi Akagi, *Fellow, IEEE*, and Jun Asakura

***Abstract*—Renewable energy sources such as wind turbine generators and photovoltaics produce fluctuating electric power. The fluctuating power can be compensated by installing an energy storage system in the vicinity of these sources. This paper describes a 6.6-kV battery energy storage system based on a cascade pulsewidth-modulation (PWM) converter with focus on a control method for state-of-charge (SOC) balancing of the battery units. A 200-V, 10-kW, 3.6-kWh (13-MJ) laboratory system combining a cascade PWM converter with nine nickel metal hydride (NiMH) battery units is designed, constructed, and tested to verify the validity and effectiveness of the proposed balancing control.**

***Index Terms*—Active-power control, battery energy storage system (BESS), cascade converter, nickel metal hydride (NiMH) battery, state-of-charge (SOC) balancing.**

I. Introduction

ENVIRONMENTAL concern and continuous depletion of fossil fuel reserves have spurred significant interest in renewable energy sources [1]. However, renewable energy sources such as wind turbine generators and photovoltaics are intermittent in nature, and produce fluctuating active power. Interconnecting these intermittent sources to the utility grid at a large scale may affect the voltage/frequency control of the grid, and may lead to severe power quality issues [2].

An energy storage system is indispensable for compensation of the active-power fluctuation, which is often referred to as "power leveling." For example, if a wind turbine generator produces a larger power than an average power over a period of time, say several seconds to 30 min, the energy storage system stores the excess power from the grid. On the other hand, if the generator produces a smaller power, it releases the shortage of power back to the grid. The energy storage system brings a significant enhancement in power quality, stability, and reliability to the grid [3].

Manuscript received October 27, 2008; revised January 14, 2009. Current version published June 10, 2009. This paper was presented at the IEEE Power Electronics Specialists Conference (PESC), Rhodes, Greece, June 15–19, 2008. Recommended for publication by Associate Editor B. Wu.

L. Maharjan and H. Akagi are with the Department of Electrical and Electronic Engineering, Tokyo Institute of Technology, Tokyo 152-8552, Japan (e-mail: laxman@akg.ee.titech.ac.jp; akagi@ee.titech.ac.jp).

S. Inoue was with the Department of Electrical and Electronic Engineering, Tokyo Institute of Technology, Tokyo 152-8552, Japan. He is now with Hitachi Ltd., Hitachi 319–1292, Japan (e-mail: shigenori.inoue@mem.iee.or.jp).

J. Asakura is with the Energy Company, Panasonic Corporation, Moriguchi 570-8677, Japan (e-mail: asakura.jun@jp.panasonic.com).

Digital Object Identifier 10.1109/TPEL.2009.2014868

A. Energy Storage Systems

Energy storage systems based on different storage devices have been investigated [3], [4]. Recently, electric double-layer capacitors (EDLCs) and batteries have emerged as promising storage devices for power system applications. An EDLC has an energy efficiency as high as 95%, a high power density of 300–500 W/kg, and a long cycle life exceeding 500 000 cycles [5]. However, EDLCs are still far lower in energy density (3–5 Wh/kg) than batteries. Although batteries have the highest energy density (50–130 Wh/kg for lithium (Li)-ion batteries and 30–80 Wh/kg for nickel metal hydride (NiMH) batteries), design engineers face a challenge to overcome their low-temperature performance and limited lifetime [6]. Moreover, they are still expensive for high-power applications. Nevertheless, both EDLCs and batteries have the potential of being used for power leveling of renewable energy sources in the near future.

Walker described a 10-MW 40-MWh battery energy storage system combining an 18-pulse voltage-source converter with lead-acid batteries [7]. The dc voltage ranged from 1750 to 2860 V. It used complicated zigzag transformers in order to synthesize a staircase voltage waveform. Miller *et al.* [8] presented a 5-MVA 2.5-MWh battery energy storage system using lead-acid batteries with a dc voltage range from 660 to 900 V. It was based on a pair of 6-pulse converters, forming a 12-pulse converter, and three 12-pulse converters were paralleled to achieve the required power rating. The transformers used in [7] and [8] would be expensive, bulky, lossy, and prone to failure. Modern multilevel converters such as diode-clamped, flying capacitor, and cascade converters are preferable to traditional transformer-based multipulse converters [9]–[14].

Although cascade converters have been primarily investigated for static synchronous compensators (STATCOMs) and motor drives [15]–[17], their prominent structure makes it suitable for energy storage applications based on EDLCs and batteries. The authors of this paper described a capacitor-based energy storage system using a cascade pulsewidth-modulation (PWM) converter with star configuration [18]. It was intended for the use with EDLCs. Attention was paid to voltage-balancing control for the dc capacitors, which was required for stable operation of the system. However, when EDLC units are replaced with battery units, state-of-charge (SOC)-balancing control would be indispensable.

B. SOC Balancing of Battery Units

The SOC of a battery is its available capacity expressed as a percentage of its maximum available capacity.

$$\text{SOC} = \frac{\text{available capacity (Ah)}}{\text{maximum available capacity (Ah)}} \times 100\%. \quad (1)$$

A battery management system (BMS) plays an important part in estimating the SOC, which is often called the "fuel gauge" function. The SOC estimation may be based on measuring some convenient parameters such as voltage, current, and internal impedance, which vary with the SOC [19]. Although it is important, the detailed explanation is beyond the scope of this paper.

Tolbert *et al.* [20] described a cascade converter using battery units for a motor drive. They used staircase modulation, and discussed a switching-pattern-swapping scheme for achieving SOC balancing of the battery units. However, no literature has presented experimental verification of SOC-balancing control for any cascade converter using multiple battery units.

This paper focuses on SOC-balancing control for a battery energy storage system based on a cascade PWM converter. The experimental system includes no voltage-balancing control because it uses nine NiMH battery units that have an almost flat charge/discharge voltage profile [21]. Voltage-balancing control may, however, be required to a practical battery energy storage system for the purpose of mitigating the undesired harmonic currents injected into the grid [22], [23]. The SOC-balancing control presented in this paper is different in form and function from the voltage-balancing control in [18]. Experimental results obtained from a 200-V, 10-kW, 3.6-kWh (13-MJ) laboratory model verify the validity and effectiveness of the SOC-balancing control. Note that although the authors discuss and verify the SOC-balancing control based on a 200-V experimental system, it can be easily expanded into the 6.6-kV system having a cascade number[1] higher than that of the experimental system. The 6.6-kV system is described in the following section to provide a basic design concept for a practical battery energy storage system.

II. Design Concept of the 6.6-kV System

Fig. 1 shows a feasible circuit configuration of the 6.6-kV energy storage system using NiMH battery units. It is based on a cascade PWM converter [9], [12]. Careful assignment of a cascade number and an operating voltage range of each battery unit are of vital importance in the system design. A transformer may be used to realize an energy storage system with a suitable cascade number and a reasonable dc voltage. As the dc voltage is lower, it is easier to achieve cell-voltage balancing[2] inside a battery unit [24]–[26]. Moreover, a design with a low cascade number enhances the system reliability and mitigates communication issues [27], [28]. Note that the transformer used is a simple step-down transformer that is easily available from the market at reasonable cost, compared to a multiwinding transformer in a conventional multipulse converter [7], [29], [30].

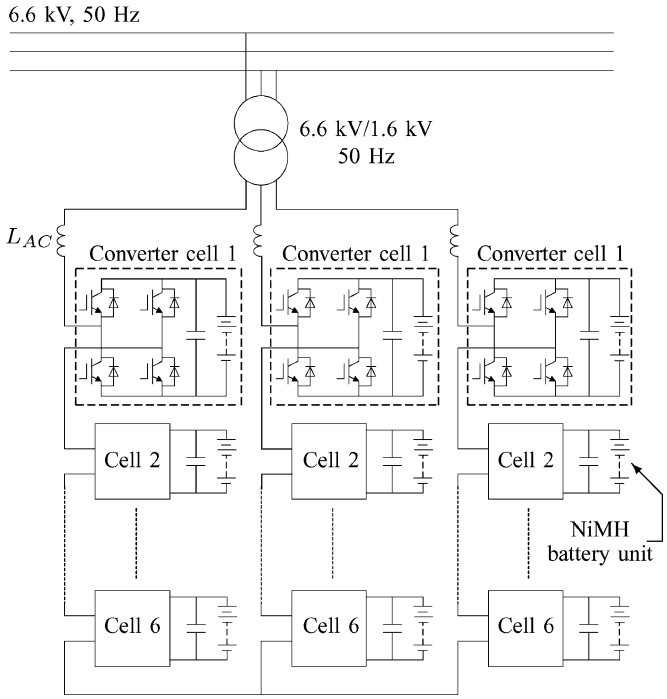

Fig. 1. Feasible circuit configuration of the 6.6-kV battery energy storage system based on a combination of a cascade PWM converter with a cascade number $N = 6$, and 18 NiMH battery units with a nominal voltage of 288 V.

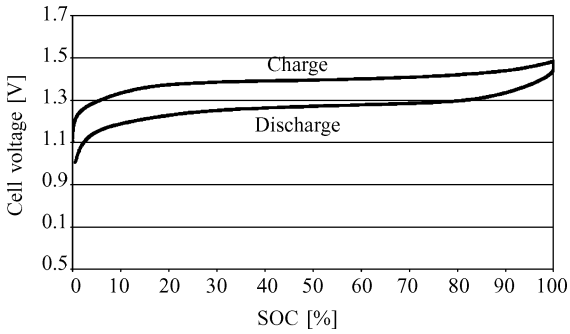

Fig. 2. Charge/discharge characteristic of a typical NiMH battery cell [21].

The so-called "asymmetrical cascade converter," characterized by battery units with different dc voltages in H-bridge converter cells, might be attractive in reducing harmonic voltage/current and switching power loss [31]. However, the authors of this paper prefer the symmetrical cascade converter to the asymmetrical one, because the use of the same battery units and converter cells brings the "modularity" to the energy storage system.

Fig. 2 shows charge and discharge characteristics of a typical NiMH battery cell [21]. A fully-charged cell measures 1.4 V and supplies a nominal voltage of 1.2 V during discharge, down to about 1.0–1.1 V. The nominal voltage of a battery unit in the 6.6-kV system may be 288 V $(= 1.2\ \text{V} \times 240\ \text{cells})$. An operating voltage of the battery unit may range from 270 to 330 V. Note that NiMH battery units with nominal voltage at

[1]The term "cascade number" implies the number of cascaded converter cells in a phase.

[2]This paper does not address cell-voltage balancing in a battery unit. It exclusively discusses SOC balancing of the multiple battery units.

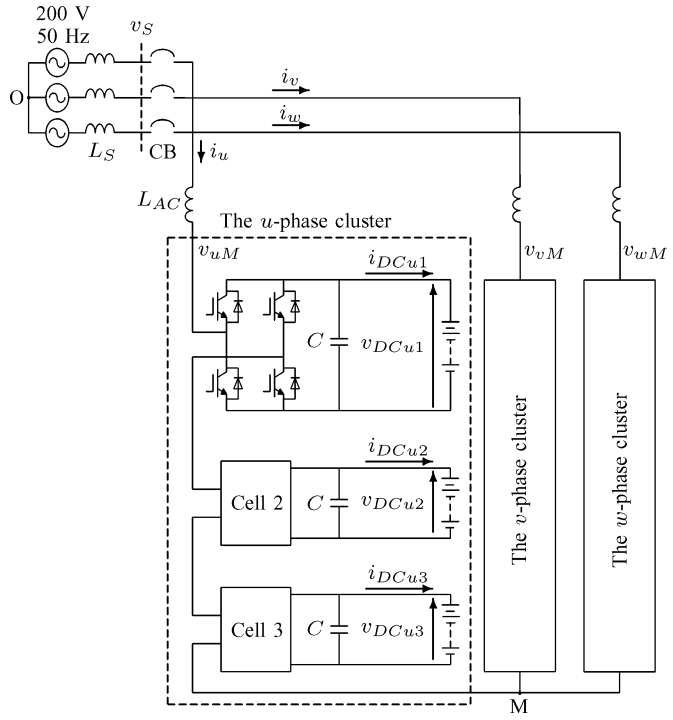

Fig. 3. Experimental system configuration of the 200-V, 10-kW, 3.6-kWh down-scaled energy storage system based on a combination of a cascade PWM converter with a cascade number $N = 3$, and nine NiMH battery units with a nominal voltage of 72 V.

TABLE I
CIRCUIT PARAMETERS OF THE EXPERIMENTAL SYSTEM RATED AT 200 V, 10 kW, AND 3.6 kWh

Nominal line-to-line rms voltage	V_S	200 V
Power rating	P	10 kW
Cascade number	N	3
AC inductor	L_{AC}	1.2 mH (10%)
Background system inductance	L_S	48 μH (0.4%)
Nominal DC voltage	V_{DC}	72 V
DC capacitor	C	16.4 mF
Unit capacitance constant	H	38 ms at 72 V
NiMH battery unit		72 V, 5.5 Ah × 9
PWM carrier frequency		800 Hz
Equivalent carrier frequency		4.8 kHz

on a three-phase, 200-V, 10-kW, 50-Hz base.

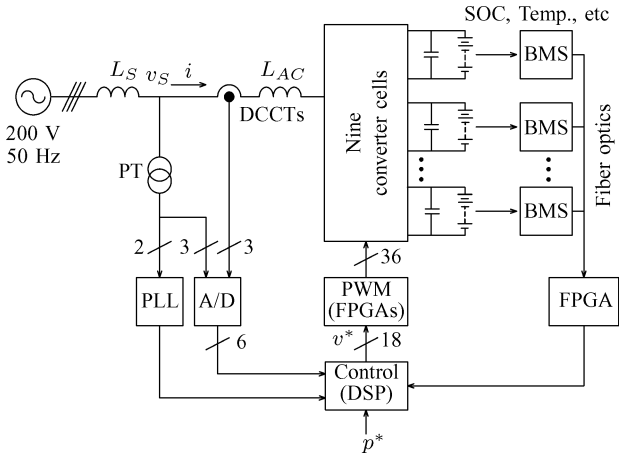

Fig. 4. Control system for the 200-V, 10-kW, 3.6-kWh battery energy storage system.

200–300 V have already been used in hybrid electric vehicles (HEVs) [32]. If the cascade number is $N = 6$, a 6.6 kV/1.6 kV transformer is required to connect the energy storage system to the 6.6-kV grid. Li-ion battery units with the same nominal voltage as 288 V$(= 3.6\ \text{V} \times 80\ \text{cells})$ are also applicable to the system.

General-purpose insulated gate bipolar transistors (IGBTs) rated at 600 V and 200 A can be used as power switching devices. The 18-converter cells are controlled by the so-called "phase-shifted unipolar sinusoidal PWM" [33]. Even though the PWM carrier frequency is set as low as 1 kHz, the equivalent carrier frequency is as high as 12 kHz $(= 2 \times 6\ \text{cells} \times 1\ \text{kHz})$. Moreover, setting such a low carrier frequency as 1 kHz brings a significant reduction in switching power loss to each converter cell. The ac voltage results in a 13-level waveform in line-to-neutral and a 25-level waveform in line-to-line, thus significantly improving the total harmonic distortion (THD) in both voltage and current.

III. 200-V, 10-kW, 3.6-kWh SYSTEM

A. System Configuration

Fig. 3 shows the system configuration of a three-phase down-scaled battery energy storage system rated at 200 V, 10 kW, and 3.6 kWh. Table I summarizes the circuit parameters. The experimental system has a cascade number $N = 3$. The battery bank consists of nine NiMH battery units that are available from Matsushita Battery Industrial Company Ltd. Each battery unit rated at 72 V and 5.5 Ah consists of a series connection of 60 cells. The total energy capacity of the battery bank consisting of the nine battery units is $W = 13$ MJ or 3.6 kWh $(= 72\ \text{V} \times 5.5\ \text{Ah} \times 9)$. The dc voltage range is from 66 to 84 V.

The nine H-bridge converter cells are controlled by the phase-shifted unipolar sinusoidal PWM with a carrier frequency of 800 Hz. The resulting line-to-neutral voltage is a seven-level waveform with an equivalent carrier frequency of 4.8 kHz $(= 2 \times 3\ \text{cells} \times 800\ \text{Hz})$.

Fig. 4 shows the control system of the 200-V system. This is based on a fully-digital main controller using a DSP and multiple field programmable gate arrays (FPGAs). Each battery unit is equipped with a BMS that provides the functions of monitoring and controlling the respective battery unit to protect it from out-of-tolerance ambient or operating conditions. Determining an SOC value of the respective battery unit is a major function of the BMS. The SOC value is needed for providing a fuel gauge indication as well as for SOC balancing of the battery units.

B. Overview of Control Strategy

Fig. 5 shows the control block diagram of the 200-V, 10-kW, 3.6-kWh energy storage system. The whole control is divided into the following two subcontrols:

1) active-power control;
2) SOC-balancing control.

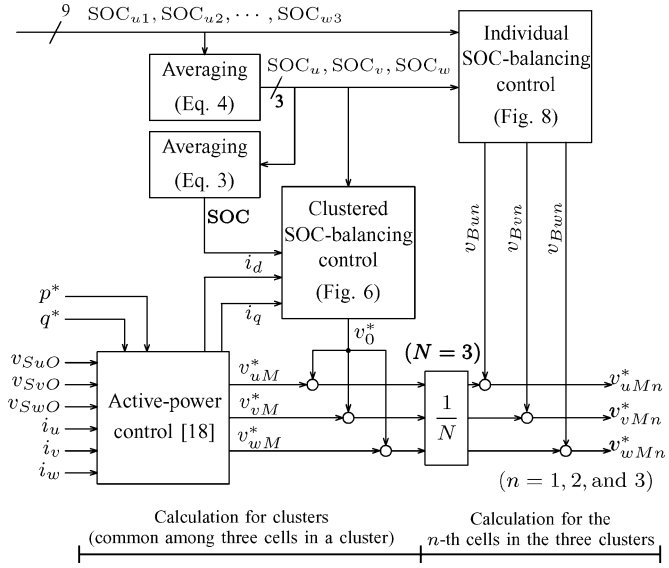

Fig. 5. Control block diagram for the 200-V system with a cascade number $N = 3$.

The active-power control is based on decoupled current control, which is the same in control method and parameters as presented in [18]. This paper thus avoids its detail explanation and focuses on the SOC-balancing control only. The SOC-balancing control is divided into "clustered SOC-balancing control" between the three clusters, and "individual SOC-balancing control" between three converter cells in each cluster. A "cluster" means a set of three converter cells connected in series in a phase.

Let $\Delta\mathrm{SOC}_u$, $\Delta\mathrm{SOC}_v$, and $\Delta\mathrm{SOC}_w$ be respective differences between the mean SOC value of the nine battery units in the three clusters and the mean SOC value of the three battery units in the u-cluster, the v-cluster, and the w-cluster.

$$\begin{bmatrix} \Delta\mathrm{SOC}_u \\ \Delta\mathrm{SOC}_v \\ \Delta\mathrm{SOC}_w \end{bmatrix} = \begin{bmatrix} \mathrm{SOC} - \mathrm{SOC}_u \\ \mathrm{SOC} - \mathrm{SOC}_v \\ \mathrm{SOC} - \mathrm{SOC}_w \end{bmatrix} \tag{2}$$

$$\mathrm{SOC} = \frac{1}{3}(\mathrm{SOC}_u + \mathrm{SOC}_v + \mathrm{SOC}_w) \tag{3}$$

$$\begin{bmatrix} \mathrm{SOC}_u \\ \mathrm{SOC}_v \\ \mathrm{SOC}_w \end{bmatrix} = \frac{1}{3}\begin{bmatrix} \mathrm{SOC}_{u1} + \mathrm{SOC}_{u2} + \mathrm{SOC}_{u3} \\ \mathrm{SOC}_{v1} + \mathrm{SOC}_{v2} + \mathrm{SOC}_{v3} \\ \mathrm{SOC}_{w1} + \mathrm{SOC}_{w2} + \mathrm{SOC}_{w3} \end{bmatrix}. \tag{4}$$

The aim of the clustered SOC-balancing control is to keep the mean SOC value of a cluster ($\mathrm{SOC}_u, \mathrm{SOC}_v$, and SOC_w) equal to the mean SOC value of the three clusters (SOC). Similarly, the aim of the individual SOC-balancing control is to keep each of the three SOC values in a cluster (for example, $\mathrm{SOC}_{u1}, \mathrm{SOC}_{u2}$, and SOC_{u3}) equal to the mean SOC value of the corresponding cluster (SOC_u).

The individual SOC-balancing control presented in this paper resembles in structure the individual voltage-balancing control presented in [17][3] and [18]. However, the clustered SOC-balancing control is different in form and function from the clustered voltage-balancing control. The clustered SOC-balancing control is based on zero-sequence-voltage injection [34] while the clustered voltage-balancing control is based on negative-sequence current injection. Moreover, the clustered SOC-balancing control has the function of balancing the three mean SOC values of the three clusters whereas the clustered voltage-balancing control has the function of balancing the three mean dc voltages of the three clusters.

[3]Reference [17] paid attention to a STATCOM, with focus on voltage balancing of dc capacitors.

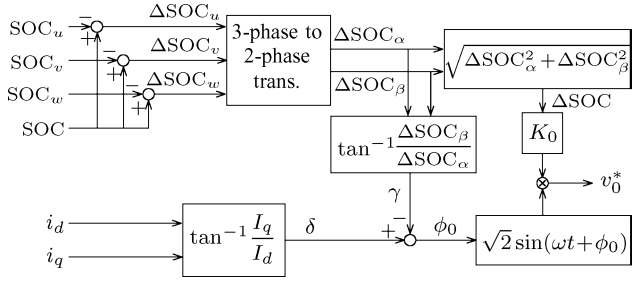

Fig. 6. Clustered SOC-balancing control based on zero-sequence-voltage injection.

IV. SOC-Balancing Control

A. Clustered SOC-Balancing Control

Fig. 6 shows the block diagram of clustered SOC-balancing control based on zero-sequence-voltage injection. The idea is to add a fundamental-frequency zero-sequence voltage v_0 to the three-phase ac voltages v_{uM}, v_{vM}, and v_{wM} of the cascade converter [34]. This allows each of the three clusters to draw or release an unequal active power without drawing negative-sequence current. Here, v_0 is the potential of point "O" with respect to point "M" in Fig. 3. Since the zero-sequence-voltage injection does not cause any change in the line-to-line voltages, the clustered SOC-balancing control produces no effect on the three-phase line currents and the total power.

If the cascade converter voltage is assumed not to contain any negative-sequence voltage, it can be expressed as

$$\begin{aligned} \begin{bmatrix} \dot{V}_{uM} \\ \dot{V}_{vM} \\ \dot{V}_{wM} \end{bmatrix} &= \begin{bmatrix} \dot{V}_{fuM} \\ \dot{V}_{fvM} \\ \dot{V}_{fwM} \end{bmatrix} + \begin{bmatrix} \dot{V}_0 \\ \dot{V}_0 \\ \dot{V}_0 \end{bmatrix} \\ &= V_{fM}\, e^{j\phi_f} \begin{bmatrix} 1 \\ e^{-j\frac{2\pi}{3}} \\ e^{j\frac{2\pi}{3}} \end{bmatrix} + V_0\, e^{j\phi_0} \begin{bmatrix} 1 \\ 1 \\ 1 \end{bmatrix} \end{aligned} \tag{5}$$

where the first term on the right-hand side represents the positive-sequence voltage with an rms magnitude of V_{fM} and a phase angle of ϕ_f with respect to the u-phase voltage. The second term represents the fundamental-frequency zero-sequence voltage with an rms magnitude of V_0 and a phase angle of ϕ_0. Both V_0 and ϕ_0 can be adjusted by the clustered SOC-balancing control.

The line currents are assumed to contain only positive-sequence currents.

$$\begin{bmatrix} \dot{I}_u \\ \dot{I}_v \\ \dot{I}_w \end{bmatrix} = I\, e^{j\delta} \begin{bmatrix} 1 \\ e^{-j\frac{2\pi}{3}} \\ e^{j\frac{2\pi}{3}} \end{bmatrix} \tag{6}$$

where

$$I = \sqrt{\frac{I_d^2 + I_q^2}{3}} \tag{7}$$

$$\delta = \begin{cases} \tan^{-1}\dfrac{I_q}{I_d}, & \text{if } I_d \neq 0 \\ \dfrac{\pi}{2}, & \text{if } I_d = 0 \quad \text{and} \quad I_q > 0 \\ -\dfrac{\pi}{2}, & \text{if } I_d = 0 \quad \text{and} \quad I_q < 0. \end{cases} \tag{8}$$

In a sinusoidal steady-state condition, I_d and I_q are equal to the d-axis current i_d and the q-axis current i_q. The u-phase power can be expressed as

$$P_u = \mathrm{Re}\left[\dot{V}_{uM} \cdot \overline{\dot{I}}_u\right] = \mathrm{Re}\left[\dot{V}_{fuM} \cdot \overline{\dot{I}}_u + \dot{V}_0 \cdot \overline{\dot{I}}_u\right]. \tag{9}$$

The first term on the right-hand side is the active power related to the positive-sequence voltage included in the u-phase ac voltage of the cascade converter, while the second term is the active power coming from the zero-sequence-voltage injection, which can be expressed as

$$\begin{bmatrix} P_{u0} \\ P_{v0} \\ P_{w0} \end{bmatrix} = V_0 I \begin{bmatrix} \cos(\phi_0 - \delta) \\ \cos\left(\phi_0 - \delta + \frac{2\pi}{3}\right) \\ \cos\left(\phi_0 - \delta - \frac{2\pi}{3}\right) \end{bmatrix}. \tag{10}$$

Equation (10) makes it clear that $P_{u0} + P_{v0} + P_{w0} = 0$. This means the zero-sequence-voltage injection produces no effect on the overall three-phase power transfer.

Let us determine the zero-sequence-voltage reference v_0^*. The SOC differences in (2) correspond to an amount of active power to be drawn or released by each of the three clusters to maintain SOC balancing among the clusters. Performing three-phase to two-phase transformation of (2) gives[4]

$$\begin{bmatrix} \Delta\mathrm{SOC}_\alpha \\ \Delta\mathrm{SOC}_\beta \\ \Delta\mathrm{SOC}_0 \end{bmatrix} = \begin{bmatrix} \sqrt{\frac{3}{2}}\Delta\mathrm{SOC}_u \\ \frac{1}{\sqrt{2}}\left(\Delta\mathrm{SOC}_v - \Delta\mathrm{SOC}_w\right) \\ 0 \end{bmatrix}. \tag{11}$$

Let $\Delta\mathrm{SOC}$ and γ be defined as

$$\begin{aligned} \Delta\mathrm{SOC} &= \sqrt{\Delta\mathrm{SOC}_\alpha^2 + \Delta\mathrm{SOC}_\beta^2} \\ &= \sqrt{\Delta\mathrm{SOC}_u^2 + \Delta\mathrm{SOC}_v^2 + \Delta\mathrm{SOC}_w^2} \end{aligned} \tag{12}$$

$$\gamma = \begin{cases} \tan^{-1}\dfrac{\Delta\mathrm{SOC}_\beta}{\Delta\mathrm{SOC}_\alpha}, & \text{if } \Delta\mathrm{SOC}_\alpha \neq 0 \\ \dfrac{\pi}{2}, & \text{if } \Delta\mathrm{SOC}_\alpha = 0 \text{ and } \Delta\mathrm{SOC}_\beta > 0 \\ -\dfrac{\pi}{2}, & \text{if } \Delta\mathrm{SOC}_\alpha = 0 \text{ and } \Delta\mathrm{SOC}_\beta < 0. \end{cases} \tag{13}$$

[4]The vector $[\mathrm{SOC}_\alpha, \mathrm{SOC}_\beta]^{\mathrm{T}}$ is not a rotating vector, but a stationary vector in alliance with the cluster having the largest SOC error.

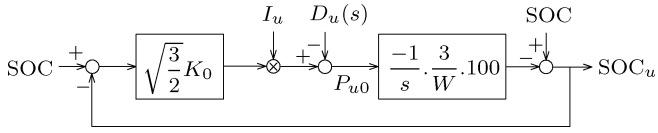

Fig. 7. Clustered SOC-balancing control, taking the u-phase as an example.

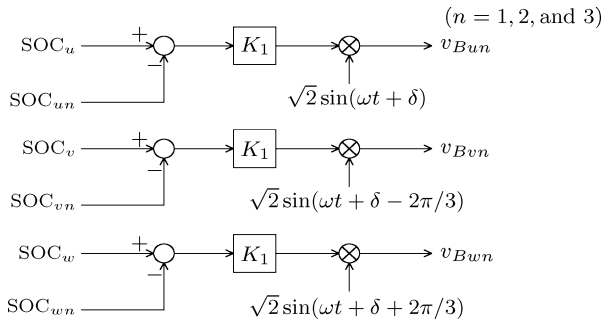

Fig. 8. Individual SOC-balancing control between three cascaded converter cells inside each cluster, paying attention to the nth-converter cells.

Here, $\Delta\mathrm{SOC}$ is a parameter representing a degree of SOC imbalance among the three clusters, while γ is a parameter associated with a distribution of SOC imbalance among the three clusters in terms of a phase angle on the α–β axes.

The zero-sequence-voltage reference is determined as

$$v_0^* = \sqrt{2} \cdot K_0 \cdot \Delta\mathrm{SOC} \cdot \sin(\omega t + \phi_0) \tag{14}$$

where K_0 is a proportional gain, and ϕ_0 is given by

$$\phi_0 = \delta - \gamma. \tag{15}$$

Phasor representation leads to

$$\dot{V}_0^* = K_0 \cdot \Delta\mathrm{SOC} \cdot e^{j\phi_0}. \tag{16}$$

Fig. 7 shows the control block diagram of clustered SOC-balancing control, taking the u-phase as an example. The coefficient $(3/W)\cdot 100$ converts a cluster battery energy (in joules) to SOC (in percentage), where $W = 13 \times 10^6$ J. The closed-loop transfer function is given by

$$\frac{\Delta\mathrm{SOC}_u(s)}{D_u(s)} = \frac{\sqrt{2/3}(1/K_0 I_u)}{1 + s\sqrt{2/3}(W/3)(1/K_0 I_u)(1/100)}. \tag{17}$$

This transfer function has a time constant given by

$$T_0 = \sqrt{\frac{2}{3}}\frac{W}{3}\frac{1}{K_0 I_u}\frac{1}{100} \tag{18}$$

where the gain K_0 was designed as

$$K_0 = 3.5\ \mathrm{V}/\%, \quad \text{at } T_0 = 6\,\mathrm{min}. \tag{19}$$

B. Individual SOC-Balancing Control

Fig. 8 shows the individual SOC-balancing control paying attention to the nth-converter cells of the three clusters. In order to determine the transfer function, let us redraw the block diagram of the individual SOC-balancing control as shown in Fig. 9, taking the u-phase nth-converter cell as an example, where $N = 3$ and $W = 13 \times 10^6$ J.

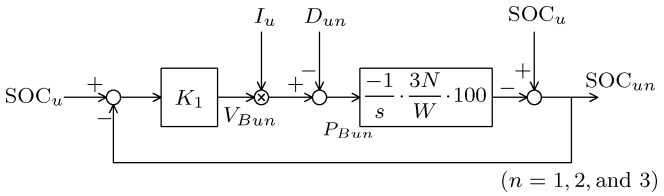

Fig. 9. Individual SOC-balancing control, taking the u-phase nth-converter cell as an example.

Let $\Delta\mathrm{SOC}_{un}$ be a difference between the mean SOC value of the u-cluster and the SOC value of the nth-converter cell in the u-cluster.

$$\Delta\mathrm{SOC}_{un} = \mathrm{SOC}_u - \mathrm{SOC}_{un} \tag{20}$$

where $n = 1$, 2, and 3. The difference $\Delta\mathrm{SOC}_{un}$ is minimized by appropriately charging or discharging the respective battery unit in the u-cluster. The superimposed ac voltage to minimize the difference is determined as

$$v_{Bun} = \sqrt{2}\cdot K_1 \cdot \Delta\mathrm{SOC}_{un} \cdot \sin(\omega t + \delta) \tag{21}$$

where K_1 is a proportional gain. Unity power factor operation makes the power factor angle δ equal to zero for charging operation, or equal to π for discharging operation.

The sum of the superimposed voltages in a cluster is equal to zero.

$$\sum_{n=1}^{N} v_{Bun} = \sqrt{2}\cdot K_1 \cdot \sin(\omega t + \delta) \cdot \sum_{n=1}^{N} \Delta\mathrm{SOC}_{un} = 0. \tag{22}$$

This shows that the individual SOC-balancing control does not interfere with the active-power control and the clustered SOC-balancing control.

The active power for achieving the SOC balancing of the u-phase nth-converter cell is given by

$$P_{Bun} = K_1 \cdot I_u \cdot \Delta\mathrm{SOC}_{un} - D_{un} \tag{23}$$

where D_{un} represents a loss or disturbance in the u-phase nth-converter cell. An amount of active power equal to P_{Bun} is drawn into, or released from, the u-phase nth-converter cell to increase or decrease the SOC_{un} value so that $\Delta\mathrm{SOC}_{un} = 0$.

$$\Delta\mathrm{SOC}_{un} = -\frac{W}{3N}\int P_{Bun}\, dt. \tag{24}$$

Note that (24) discards a 100-Hz component[5] from p_{Bun} $(= v_{Bun}\cdot i_u)$. Equations (20), (23), and (24) result in Fig. 9. The closed-loop transfer function is given by

$$\frac{\Delta\mathrm{SOC}_{un}(s)}{D_{un}(s)} = \frac{(1/K_1 I_u)}{1 + s(W/3N)(1/K_1 I_u)(1/100)}. \tag{25}$$

This transfer function has a time constant given by

$$T_1 = \frac{W}{3N}\frac{1}{K_1 I_u}\frac{1}{100}. \tag{26}$$

[5]The 100-Hz component included in p_{Bun} makes no contribution to charging or discharging the battery unit, because its mean value is zero over one fundamental frequency cycle (20 ms). Moreover, a high-energy density of the battery unit makes the effect of the 100-Hz component on the SOC negligible.

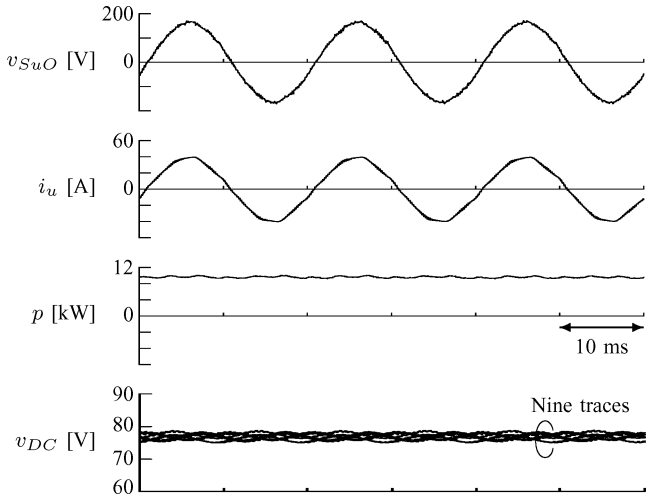

Fig. 10. Experimental waveforms when the battery bank was charged at 10 kW with a mean SOC window between 40% and 45%.

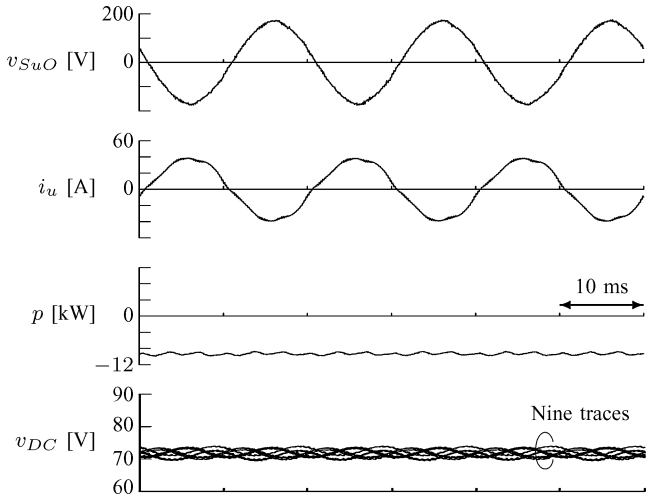

Fig. 11. Experimental waveforms when the battery bank was discharged at 10 kW with a mean SOC window between 40% and 45%.

Finally, the gain K_1 was designed as

$$K_1 = 0.7\ \mathrm{V}/\%, \quad \text{at } T_1 = 12\ \mathrm{min}. \tag{27}$$

V. Experimental Results

A. Charging and Discharging Waveforms

Fig. 10 shows the experimental waveforms when the battery bank was charged up at the rated power of 10 kW. The waveforms of v_{SuO} and i_u were in phase because this system was operated with a condition of $q^* = 0$. The u-phase current was slightly distorted with a current THD of 3.5% at a battery-unit voltage of 78 V.

Fig. 11 shows the experimental waveforms when the battery bank was discharged down at the rated power of 10 kW. The waveforms of v_{SuO} and i_u were out of phase by 180°. The u-phase current had a THD of 5.4%. The THD value is expected to be lower in the 6.6-kV system because a saturation/forward voltage ($\simeq$2 V) of 1.2-kV IGBTs/diodes is much lower than a

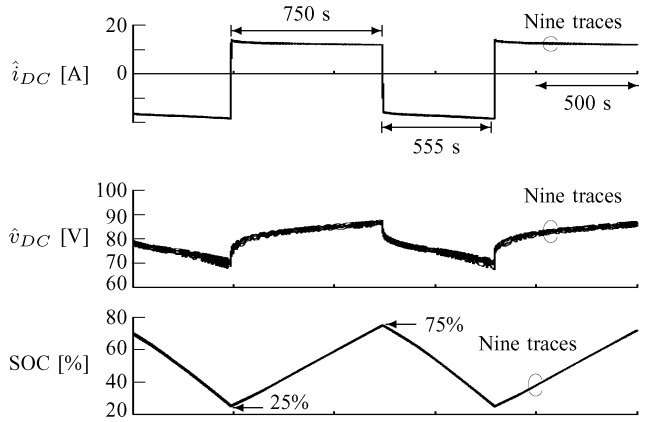

Fig. 12. Experimental waveforms with repetitive charging and discharging of the battery bank, where a mean SOC window was kept between 25% and 75%.

battery-unit voltage ranging from 600 to 750 V with a higher equivalent carrier frequency. The mean SOC window was in between 40% and 45% when these charge–discharge waveforms were observed.

Fig. 12 shows the experimental waveforms when the battery bank was repetitively charged up to a mean SOC of 75% and discharged down to a mean SOC of 25%. Although the experiment used a mean SOC window between 25% and 75%, a wider window, for example, from 10% to 90%, may be used in an actual system. Note, however, that NiMH batteries show extended cycle life with a lower depth-of-discharge (DOD)[6] value [6]. Here, $\hat{i}_{\rm dc}$, $\hat{v}_{\rm dc}$, and SOC were obtained from a BMS with a sampling rate of 1 $\rm s^{-1}$. Since the power was set at $p = \pm 10$ kW, the charging or discharging battery current was observed to be around 15 A. This is equivalent to a C-rate[7] of 2.7 C $(= 15\rm A/5.5\ Ah)$.

B. Battery-Unit Voltage and Current Waveforms

Fig. 13 shows the voltage and current waveforms of a battery unit in the u-cluster, where (a) corresponds to those during charging $(p = 10\ \rm kW)$, while (b) to those during discharging $(p = -10\ \rm kW)$ both at a mean SOC value of 65%. The waveform of v_{DCu1} contained a 100-Hz component of 2 V (peak-to-peak), and the waveform of i_{DCu1} contained a 100-Hz component of 17.5 A (peak-to-peak) during charging. They are in phase so that the internal impedance of the battery unit can be considered purely resistive. The internal resistance is estimated to be 115 m$\Omega(=2\ \rm V/17.5A)$. The dc internal resistance of a stand-alone battery unit was measured to be 133 mΩ at an SOC value of 65% and a battery temperature of $30\,^\circ$C.

C. Transient Waveforms

Fig. 14 shows transient waveforms from charging to discharging operation with a ramp change in active power from 10 to -10 kW in 30 ms with a mean SOC value of around 70%. Fig. 15

[6]DOD is a measure of energy withdrawn from a battery, expressed as a percentage of the full capacity.

[7]The term "C-rate" is a charging or discharging rate of a battery expressed in terms of its total storage capacity in ampere-hour. A rate of 1 C means a complete transfer of the stored energy in 1 h.

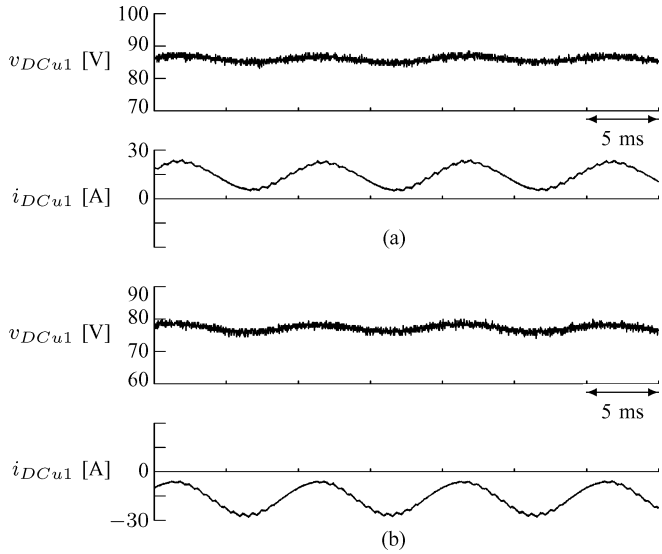

Fig. 13. Battery voltage and current waveforms: (a) during charging at 10 kW; (b) during discharging at 10 kW. The mean SOC value was 65%.

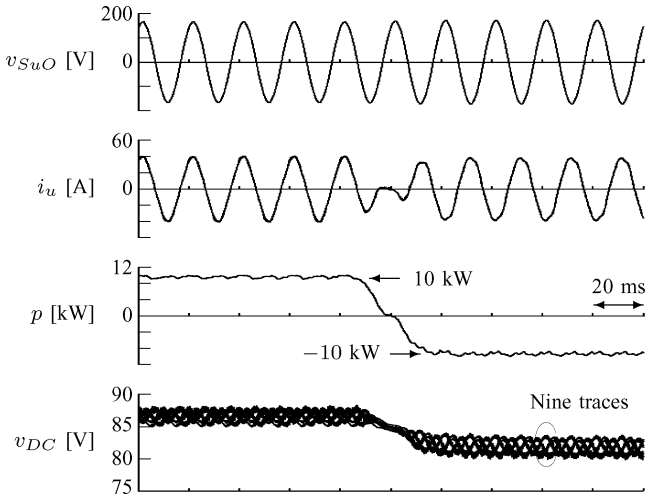

Fig. 14. Experimental waveforms when p^* was changed from 10 kW to -10 kW in 30 ms with a mean SOC value of 70%.

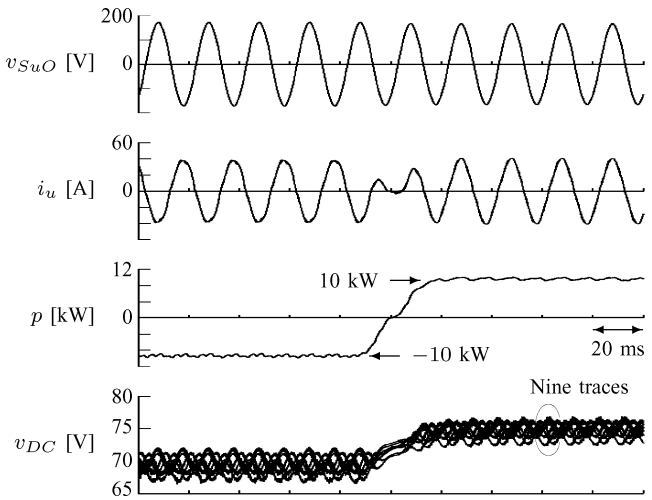

Fig. 15. Experimental waveforms when p^* was changed from -10 to 10 kW in 30 ms with a mean SOC value of 30%.

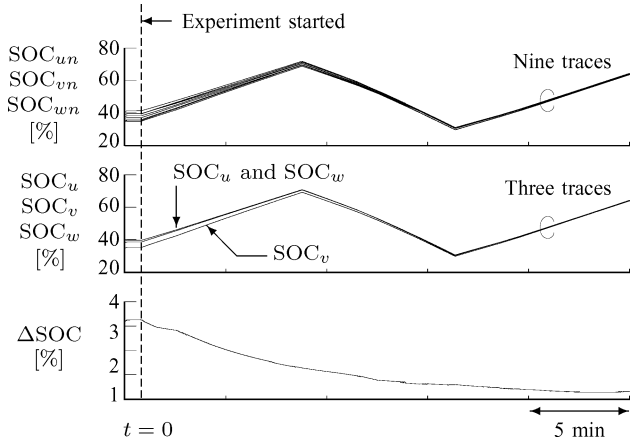

Fig. 16. Experimental waveforms to verify the effectiveness of the SOC-balancing control, where a mean SOC value was kept between 30% and 70% with $p^* = 10$ kW and $q^* = 0$.

shows transient waveforms from discharging to charging operation with a ramp change in active power from -10 to 10 kW in 30 ms with a mean SOC value of around 30%. These waveforms confirmed stable operation even in the transient states.

D. Effectiveness of the SOC-Balancing Control

The SOC-balancing control is introduced to make equal all the SOC values of the nine battery units for the effective use of the battery-bank energy. In Fig. 16, the upper part shows all the nine SOC values of the battery units, the middle part shows the three mean SOC values of the u-, v-, and w-clusters, and the lower part shows the value of $\Delta\mathrm{SOC}$ defined in (12).

Before starting the experiment $(t = 0)$, the SOC values of the nine battery units had a maximal imbalance of 5% between the lowest and highest ones. However, when the SOC-balancing control was started along with $p^* = \pm 10$ kW at $t = 0$, the nine SOC values gradually started to converge together. In about 15 mins, all the SOC values were effectively balanced. The value of $\Delta\mathrm{SOC}$ was reduced to one-third of its initial value in about 7 min. This fact agreed well with $T_0 = 6$ min in (19).

VI. Conclusion

This paper has described a 6.6-kV battery energy storage system using a cascade PWM converter, with focus on a control method for SOC balancing of the multiple battery units. Experimental results obtained from a 200-V, 10-kW, 3.6-kWh laboratory model using nine NiMH battery units have verified the effectiveness of the proposed control method.

References

[1] S. R. Bull, "Renewable energy today and tomorrow," *Proc. IEEE*, vol. 89, no. 8, pp. 1216–1226, Aug. 2001.
[2] R. D. Richardson and G. M. McNerney, "Wind energy systems," *Proc. IEEE*, vol. 81, no. 3, pp. 378–389, Mar. 1993.
[3] P. F. Ribeiro, B. K. Johnson, M. L. Crow, A. Arsoy, and Y. Liu, "Energy storage systems for advanced power applications," *Proc. IEEE*, vol. 89, no. 12, pp. 1744–1756, Dec. 2001.
[4] A. Rufer and P. Barrade, "A supercapacitor-based energy-storage system for elevators with soft commutated interface," *IEEE Trans. Ind. Appl.*, vol. 38, no. 5, pp. 1151–1159, Sep./Oct. 2002.
[5] A. Burke, "Ultracapacitors: Why, how, and where is the technology," *J. Power Sources*, vol. 91, no. 1, pp. 37–50, Nov. 2000.
[6] U. Kohler, J. Kumpers, and M. Ullrich, "High performance nickel-metal hydride and lithium-ion batteries," *J. Power Sources*, vol. 105, no. 2, pp. 139–144, Mar. 2002.
[7] L. H. Walker, "10-MW GTO converter for battery peaking service," *IEEE Trans. Ind. Appl.*, vol. 26, no. 1, pp. 63–72, Jan./Feb. 1990.
[8] N. W. Miller, R. S. Zrebiec, R. W. Delmerico, and G. Hunt, "Design and commissioning of a 5-MVA, 2.5-MWh battery energy storage," in *Proc. Conf. Rec. IEEE Transm. Distrib. Conf.*, Sep. 1996, pp. 339–345.
[9] R. H. Baker and L. H. Bannister, "Electric power converter," U.S. Patent 3 867 643, Feb. 1975.
[10] R. H. Baker, "Bridge converter circuit," U.S. Patent 4 270 163, May 1981.
[11] A. Nabae, I. Takahashi, and H. Akagi, "A new neutral-point-clamped PWM inverter," *IEEE Trans. Ind. Appl.*, vol. IA-17, no. 5, pp. 518–523, Sep./Oct. 1981.
[12] M. Marchesoni, M. Mazzucchelli, and S. Tenconi, "A nonconventional power converter for plasma stabilization," *IEEE Trans. Power Electron.*, vol. 5, no. 2, pp. 212–219, Apr. 1990.
[13] T. A. Meynard and H. Foch, "Multi-level conversion: High voltage choppers and voltage-source inverters," in *Proc. IEEE PESC*, 1992, vol. 1, pp. 397–403.
[14] J. S. Lai and F. Z. Peng, "Multilevel converters—A new breed of power converters," *IEEE Trans. Ind. Appl.*, vol. 32, no. 3, pp. 509–517, May/Jun. 1996.
[15] P. W. Hammond, "A new approach to enhance power quality for medium voltage ac drives," *IEEE Trans. Ind. Appl.*, vol. 33, no. 1, pp. 202–208, Jan./Feb. 1997.
[16] R. H. Osman, "A medium-voltage drive utilizing series-cell multilevel topology for outstanding power quality," in *Conf. Rec. IEEE IAS Annu. Meet.*, 1999, vol. 4, pp. 2662–2669.
[17] H. Akagi, S. Inoue, and T. Yoshii, "Control and performance of a transformerless cascade PWM STATCOM with star configuration," *IEEE Trans. Ind. Appl.*, vol. 43, no. 4, pp. 1041–1049, Jul./Aug. 2007.
[18] L. Maharjan, T. Yoshii, S. Inoue, and H. Akagi, "A transformerless energy storage system based on a cascade multilevel PWM converter with star configuration," *IEEE Trans. Ind. Appl.*, vol. 44, no. 5, pp. 1621–1630, Sep./Oct. 2008.
[19] S. Piller, M. Perrin, and A. Jossen, "Methods for state-of-charge determination and their applications," *J. Power Sources*, vol. 96, no. 1, pp. 113–120, Jun. 2001.
[20] L. M. Tolbert, F. Z. Peng, and T. G. Habetler, "Multilevel converters for large electric drives," *IEEE Trans. Ind. Appl.*, vol. 35, no. 1, pp. 36–44, Jan./Feb. 1999.
[21] J. J. C. Kopera, *Inside the Nickel Metal Hydride Battery*. Orion, MI: Cobasys, Jun. 2004.
[22] Q. Song, W. Liu, Z. Yuan, W. Wei, and Y. Chen, "DC voltage balancing technique using multi-pulse optimal PWM for cascade H-bridge inverters based STATCOM," in *Proc. IEEE PESC*, 2004, vol. 6, pp. 4768–4772.
[23] D. Soto and T. C. Green, "A dc link capacitor voltages control strategy for a PWM cascade STATCOM," in *Proc. IEEE PESC*, 2005, pp. 2251–2256.
[24] S. T. Hung, D. C. Hopkins, and C. R. Mosling, "Extension of battery life via charge equalization control," *IEEE Trans. Ind. Electron.*, vol. 40, no. 1, pp. 96–104, Feb. 1993.
[25] N. H. Kutkut, D. M. Divan, and D. W. Novotny, "Charge equalization for series connected battery strings," *IEEE Trans. Ind. Appl.*, vol. 31, no. 3, pp. 562–568, May/Jun. 1995.
[26] K. Nishijima, H. Sakamoto, and K. Harada, "A PWM controlled simple and high performance battery balancing system," in *Proc. IEEE PESC*, 2000, vol. 1, pp. 517–520.
[27] P. C. Loh, D. G. Holmes, and T. A. Lipo, "Implementation and control of distributed PWM cascaded multilevel inverters with minimal harmonic distortion and common-mode voltage," *IEEE Trans. Power Electron.*, vol. 20, no. 1, pp. 90–99, Jan. 2005.
[28] J. Rodriguez, P. W. Hammond, J. Pontt, R. Musalem, P. Lezana, and M. J. Escobar, "Operation of a medium-voltage drive under faulty conditions," *IEEE Trans. Ind. Electron.*, vol. 52, no. 4, pp. 1080–1085, Aug. 2005.
[29] S. Mori, K. Matsuno, M. Takeda, and M. Seto, "Development of a large static var generator using self-commutated inverters for improving power system stability," *IEEE Trans. Power Syst.*, vol. 8, no. 1, pp. 371–377, Feb. 1993.

[30] C. Schauder, M. Gernhardt, E. Stacey, T. Lemak, L. Gyugyi, T. W. Cease, and A. Edris, "Development of a ±100 MVAr static condenser for voltage control of transmission systems," *IEEE Trans. Power Del.*, vol. 10, no. 3, pp. 1486–1496, Jul. 1995.
[31] J. Rodriguez, J. S. Lai, and F. Z. Peng, "Multilevel inverters: a survey of topologies, controls, and applications," *IEEE Trans. Ind. Electron.*, vol. 49, no. 4, pp. 724–738, Aug. 2002.
[32] C. C. Chan, "The state of the art of electric, hybrid, and fuel cell vehicles," *Proc. IEEE*, vol. 95, no. 4, pp. 704–718, Apr. 2007.
[33] Y. Liang and C. O. Nwankpa, "A new type of STATCOM based on cascading voltage-source inverters with phase-shifted unipolar SPWM," *IEEE Trans. Ind. Appl.*, vol. 35, no. 5, pp. 1118–1123, Sep./Oct. 1999.
[34] R. E. Betz, T. Summers, and T. Furney, "Symmetry compensation using a H-bridge multilevel STATCOM with zero sequence injection," in *Conf. Rec. IEEE IAS Annu. Meet.*, 2006, pp. 1724–1731.

Laxman Maharjan (S'06) was born in Lalitpur, Nepal, on January 2, 1979. He received the B.E. degree in electrical engineering from Tribhuvan University, Institute of Engineering, Kathmandu, Nepal, in 2002, and the M.S. degree in electrical engineering in 2007 from Tokyo Institute of Technology, Tokyo, Japan, where he has been working toward the Ph.D. degree.

He was a Research Student at Tokyo Institute of Technology from October 2004 to March 2005. His current research interests include cascade multilevel converters and energy storage systems.

Shigenori Inoue (S'02–M'07) was born in Fujimi, Saitama, Japan, on January 29, 1979. He received the B.S. and M.S. degrees from Tokyo Metropolitan University, Tokyo, Japan, in 2002 and 2004, respectively, and the Ph.D. degree from Tokyo Institute of Technology, Tokyo, in 2007.

Since April 2008, he has been with Hitachi Ltd. His current research interests include medium-voltage power conversion systems, bidirectional isolated dc/dc converters, SiC/GaN-based power devices, and active power filters.

From April 2007 to March 2008, he was a Research Fellow of Japan Society for the Promotion of Science (JSPS).

Hirofumi Akagi (M'87–SM'94–F'96) was born in Okayama, Japan, on August 19, 1951. He received the B.S. degree from Nagoya Institute of Technology, Nagoya, Japan, in 1974, and the M.S. and Ph.D. degrees from the Tokyo Institute of Technology, Tokyo, Japan, in 1976 and 1979, respectively, all in electrical engineering.

During 1979, he was an Assistant Professor with Nagaoka University of Technology, Nagaoka, Japan, where he later became an Associate Professor in the Department of Electrical Engineering. For a period of ten months during 1987, he was a Visiting Scientist at Massachusetts Institute of Technology (MIT), Cambridge, where he was also a Visiting Professor from June to August in 1996. From 1991 to 1999, he was a Professor in the Department of Electrical Engineering, Okayama University, Okayama. From March to May 1996, he was a Visiting Professor at the University of Wisconsin, Madison. Since January 2000, he has been a Professor in the Department of Electrical and Electronic Engineering, Tokyo Institute of Technology. He has been a keynote or an invited speaker at international conferences. He has authored or coauthored more than 80 IEEE TRANSACTIONS papers, and two invited papers published in the PROCEEDINGS OF THE IEEE. The total citation index for his papers in *Google Scholar* is more than 7000. His current research interests include power conversion systems, ac motor drives, active and passive electromagnetic interference (EMI) filters, high-frequency resonant inverters for induction heating and corona discharge treatment processes, and utility applications of power electronics such as active filters, self-commutated back-to-back (BTB) systems, and flexible ac transmission system (FACTS) devices.

Dr. Akagi was elected as a Distinguished Lecturer of the IEEE Power Electronics Society and the IEEE Industry Applications Society for 1998–1999. He received two IEEE Transactions on Industry Applications Prize Paper Awards in 1991 and 2004, two IEEE Transactions on Power Electronics Prize Paper Awards in 1999 and 2003, nine IEEE Industry Applications Society Committee Prize Paper Awards, the 2001 IEEE William E. Newell Power Electronics Award, the 2004 IEEE Industry Applications Society Outstanding Achievement Award, and the 2008 IEEE Richard H. Kaufmann Technical Field Award. He served as the President of the IEEE PELS for 2007–2008.

Jun Asakura was born in August 1975. He received the M.S. degree in electrical, electronic, and information engineering from Osaka University, Osaka, Japan, in 2000.

Since April 2004, he has been with Panasonic Corporation, Moriguchi, Japan, formerly known as Matsushita Electric Industrial Company Ltd.